JOURNAL OF CATALYSIS **172,** 488–493 (1997)
ARTICLE NO. CA971899

RESEARCH NOTE

Fe^{3+} Exchanged Mesoporous Al-HMS and Al-MCM-41 Molecular Sieves for Selective Catalytic Reduction of NO with NH_3

Ralph T. Yang,* Thomas J. Pinnavaia,† Weibin Li,* and Wenzhong Zhang†

*Department of Chemical Engineering, University of Michigan, Ann Arbor, Michigan 48109-2136; and †Department of Chemistry, Michigan State University, East Lansing, Michigan 48824

Received July 28, 1997; revised September 8, 1997; accepted September 9, 1997

Selective catalytic reduction (SCR) of nitrogen oxides with ammonia is of increasing industrial importance. The present commercial catalysts are V_2O_5 mixed with WO_3 and/or MoO_3 supported on TiO_2 (1). The drawbacks for vanadium oxide catalysts are significant side-reaction such as SO_2 oxidation to SO_3, as well as high cost for disposal of the spent catalyst due to high toxicity. Therefore, there is a need to improve the design of catalyst for the SCR reaction.

Iron oxide is among the most selective and active catalysts with low activity for SO_2 oxidation and low cost for disposal of the used catalysts. For the Fe_2O_3-based catalysts micropore diffusion resistance plays a role in the overall reaction rates (2, 3). Iron oxide pillared clays (Fe_2O_3-PILC) (4) have been used for the NO SCR reaction (3, 5, 6). Despite diffusion limitation that almost certainly operates in these systems, these Fe_2O_3-PILC materials have been shown to have remarkably high SCR activities (3, 5, 6). Improving access to the iron centers by supporting them on a mesoporous carrier should greatly improve SCR activity.

MCM-41 is one of a new family of mesoporous silicate molecular sieves with a hexagonal arrangement of unidimensional channels with uniform sizes in the range of 20 to 100 Å (7, 8). It has already attracted considerable industrial and academic interest (9–12). HMS is another type of hexagonal mesoporous silica molecular sieve which is distinguishable from MCM-41 in part by its smaller domain size with shorter channels and larger textural mesoporosity (13). These features of HMS may provide better transport channels for reactants to access the active centers than its MCM-41 analog.

In the present work we investigate the NO SCR activity of Fe^{3+} exchanged forms of Al-MCM-41 and Al-HMS. The activities of NO SCR reaction over Fe^{3+}-ion exchanged Al-MCM-41 and Al-HMS, as well as Fe_2O_3-PILC were comparatively studied. The results show that Fe/Al-HMS exhibits substantially higher activities over Fe/Al-MCM-41. The results were interpreted in terms of pore diffusivity analysis.

In order to minimize the number of factors which may cause significant differences in the catalytic properties between Al-MCM-41 and Al-HMS, the aluminum contents of both molecular sieves were controlled to around 8%. Also the pore size distribution for the two supports was controlled to around 28 Å. Al-MCM-41 was prepared using tetraethyl orthosilicate (TEOS) as the silicon precursor and cetyltrimethyl ammonium bromide as the surfactant template. NaOH and $Al_2(SO_4)_3$ in aqueous solution were mixed together. Then surfactant was added and dispersed uniformly. Next, the TEOS was added under vigorous stirring for 2 h at ambient temperature. The molar ratio of reactants in this mixture was 1 Si : 0.08 Al : 0.2 Surf. : 0.5 NaOH : 150 H_2O. This reaction mixture was then transferred into an autoclave and allowed to age at 100°C for 4 days. The white reaction product was filtered, washed thoroughly with water, and dried at ambient temperature. The surfactant in the product was removed by calcination at 540°C for 6 h. The heating rate used was 2°C/min.

Al-HMS was prepared using TEOS as the silicon source, dodecylamine as the surfactant template, aluminum sec-butoxide as the aluminum precursor, and ethanol as the co-solvent. The molar ratio of the reactants was 1 Si : 0.08 Al : 0.28 Surf : 21 EtOH : 5 BuOH : 33 H_2O. The solution of surfactant in ethanol was added to water to make a clear solution. Then, a preheated (80°C for 3 h) clear solution of aluminum butoxide and TEOS in sec-butanol (BuOH) was slowly added to the surfactant solution under vigorous stirring at ambient temperature for 24 h in a fume hood. The reaction mixture was left uncovered in order to concentrate the product by solvent evaporation. The resulting slurry was filtered and dried in air at ambient temperature. Finally, the templating surfactant was removed by calcination at 540°C for 6 h.

Powder X-ray diffraction patterns of Al-MCM-41 and Al-HMS were measured on a Rigaku Rotaflex diffractometer equipped with a rotating anode under 45 kV and

0021-9517/97 $25.00

100 mA and Cu K_α radiation ($\lambda = 1.542$ Å). The scattering and receiving slits were 1/6 and 0.3°, respectively.

N_2 adsorption and desorption isotherms at −196°C were carried out on a Coulter Omnisorp 360CX sorptometer under a continuous mode. The pore size distribution was calculated from the N_2 adsorption branch using Horvath–Kawazoe model (4).

Transmission electron microscopy (TEM) studies were conducted on a JEOL 100CX instrument using an electron beam generated by a field emission type CeB6 gun and an acceleration voltage of 120 kV. The resolution of this instrument was about 6 Å measured by indirect measurement of the spherical aberration constant (15) under medium high magnification (i.e., ×100,000). Therefore, it was possible to resolve pores with a size at about 30 Å. The specimen was prepared by dipping a carbon film covered copper grid into a suspension (0.1 wt%) of mesoporous materials in ethanol that was presonicated for 10 min. Thin-section methods were not used because texture–pore information was lost after thin-sectioning.

Fe^{3+} exchange for Na^+ in Al-MCM-41 and for H^+ in Al-HMS was carried out by using 0.2 M aqueous $Fe(NO_3)_3$ solution at pH 1.7 and ambient temperature for 24 h. The resulting materials were filtered, dried at 110°C and calcined at 450°C in air. Then they were denoted as Fe/Al-MCM-41 and Fe/Al-HMS, respectively.

Fe^{3+} ion exchanged and calcined samples were used as catalysts for SCR reaction. Typical reaction conditions were as follows: 1000 ppm of NO, 1000 ppm of NH_3, and 2% O_2 in helium. The total flow rate was 500 ml/min over a catalyst weight of 0.40 g. The quartz tube reactor system for the SCR reaction was the same as described elsewhere (3). The reactor temperature was controlled by an Omega (CN-2010) programmable temperature controller. The powder catalyst was supported on a fritted support. Two sets of flowmeters were employed for blending a synthetic flue gas. Rotameters were used to control high flow rates (i.e., He, NH_3 + He, and NO + He). Mass flowmeters were used for gases (i.e., O_2) with low flow rates. The premixed gases (1.0% NO and 1.0% NH_3 in helium) were supplied by Matheson. To prevent deposition of ammonium sulfate, the tubing leading to the reactor was heated by a heating tape. The NO concentration was continuously monitored by a chemiluminescent NO/NO_x analyzer (Thermo Electron Corporation, Model 10). To avoid any analytical error caused by oxidation of ammonia in the converter of the NO/NO_x analyzer, an ammonia trap (phosphoric acid solution) was installed before the sample inlet to the analyzer.

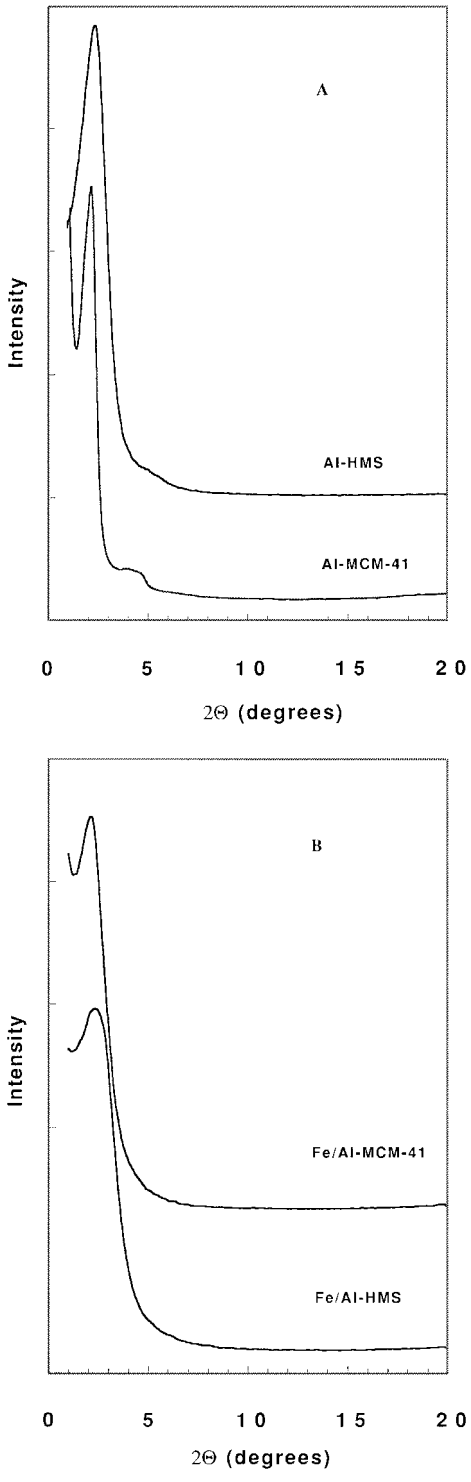

FIG. 1. Powder XRD patterns (Cu K_α) for (A) calcined (540°C) Al-HMS and Al-MCM-41; (B) Fe^{3+} ion exchanged catalysts after use as catalysts for NO reduction by NH_3.

CATALYST CHARACTERIZATION

Figure 1a shows the X-ray powder diffraction patterns of Al-HMS and Al-MCM-41. Obviously, Al-HMS exhibits a substantially broader (100) reflection peak than the Al-MCM-41 analog, due primarily to the smaller crystallite domain size. The tabulated physical parameters in Table 1 show that both Al-HMS and Al-MCM-41 had similar pore sizes and BET surface areas. Both catalysts

TABLE 1

Physical Properties of Al-HMS and Al-MCM-41[a]

Parameters	d_{100} (Å)	H-K pore size (Å)	S_{BET} (m^2/g)
Al-MCM-41	39.2 (39.5)	29 (24)	851 (763)
Al-HMS	37.0 (37.3)	27 (23)	799 (732)

[a] The data in parentheses are for the used Fe-ion exchanged catalysts after SCR reaction.

contained about 8 mol% of Al as analyzed by means of ICP atomic emission spectrometry, and their (100) reflections remained after the SCR reaction (Fig. 1b). Figure 2 shows TEM images of the HMS sample. The textural pores of HMS which are clearly seen in Fig. 2a, were formed through encompassing cross-linked domains. The sizes of the textural pores (holes) ranged from 150 to 400 Å. The same area observed under much higher magnifications revealed uniform framework mesopores with a pore size of about 30 Å. This value is close to the Horvath–Kawazoe pore size (27 Å). No textural pores were seen for Al-MCM-41 using TEM. The lack of textural porosity is in good agreement with the N_2 adsorption and desorption results and consistent with previously reported studies that compared the crystallite domain size of MCM-41 to that of HMS (13).

OVERALL SCR ACTIVITIES

The NO conversions for SCR by NH_3 on the Fe/Al-MCM-41 and Fe/Al-HMS are shown as functions of temperature in Fig. 3. Measurements were also made on Al-MCM-41 (without Fe^{3+} ion exchange). No NO conversion was detectable at all temperatures tested (up to 400°C). Compared to the V_2O_5-based catalysts; i.e., V_2O_5/TiO_2 (16) and $V_2O_5 + WO_3/TiO_2$ (17), both Fe/Al-MCM-41 and Fe/Al-MCM-41 catalysts showed a wider temperature window, which is a desirable feature for practical applications.

From the conversion data and the reaction conditions, one may calculate the rate constants. For a plug-flow integral reactor, for a first-order (with respect to NO) reaction, and under diffusion resistance-free conditions, the rate constant k is given by

$$k = -\frac{F_0}{[NO]_0 W}\ln(1 - X), \qquad [1]$$

where F_0 is the molar NO feed rate, $[NO]_0$ is the molar NO concentration at the inlet (at the reaction temperature), W is the catalyst amount, and X is the fractional NO conversion.

For the NH_3 SCR reaction on Fe_2O_3 catalysts, it has been shown that the reaction is first-order with respect to NO (2); i.e.,

$$\text{Rate} = -k[NO]. \qquad [2]$$

Since the reaction is heterogeneous, three meaningful rate expressions are gmol/s per g catalyst, gmol/s per surface area, or gmol/s per active site (if the active sites are known). Since Fe^{3+} is the active site, it is possible to express the rate based on per site. Moreover, the first-order rate constant calculated from Eq. [1] is an apparent rate constant since Eq. [1] is based on the assumption of being free of pore-diffusion resistance.

The apparent rate constants for the Fe/Al-MCM-41 and Fe/Al-HMS catalysts are given in Table 2, on the basis of both per gram and per Fe^{3+} site. It is meaningful to compare these rate constants with those on other forms of Fe^{3+} catalysts. Fe_2O_3-pillared clays have been shown to have high SCR activities, including Fe_2O_3-pillared clay (5) and a delaminated form (18) of Fe_2O_3-pillared clay (3). The early work of Wong and Nobe (2) showed high activities by the supported Fe_2O_3 (on TiO_2 and Al_2O_3) (2). The rate constants on these Fe^{3+}-based catalysts are compared in Table 2.

For the pillared clays, it is reasonable to assume 100% dispersion for Fe^{3+} due to the small dimensions of the Fe_2O_3 pillars (3). For Fe_2O_3 supported on TiO_2 and Al_2O_3 (2), the amount of Fe_2O_3 was 20% by weight, which was more than enough to fully cover the respective surfaces (surface area = 46 m^2/g for TiO_2 and 200 m^2/g for Al_2O_3) (2). Hence it is reasonable to assume that the surfaces were fully covered by Fe_2O_3. The Fe^{3+} site densities on these catalysts were estimated by assuming close-packing, i.e., 0.2 g/100 m^2 (19). In the study of Wong and Nobe (2), their reactant gas composition was the same as that used in this study. Their catalyst amount was 14 g and the gas flow rate was 300 liters NTP/h. So a conversion, based on first-order reaction (2) and plug-flow reactor, was needed for our comparison.

TABLE 2

Apparent Rate Constants (Assuming No Diffusion Limitation), k, for NH_3 SCR on Different Iron Catalysts

		k ($cm^3/g/s$)		$k \times 10^{20}$ ($cm^3/Fe^{3+}/s$)	
Catalyst	Fe^{3+}/g	350°C	400°C	350°C	400°C
Fe/Al-HMS	1.6×10^{20} [a]	34.6	53.5	21.9	33.9
Fe/Al-MCM-41	1.3×10^{20} [a]	22.7	29.1	16.9	21.7
Delam. Fe_2O_3-PILC	1.2×10^{21} [b]	137	176	11.4	14.7
Fe_2O_3-PILC	3.8×10^{20} [b]	40	53	10.5	13.9
Fe_2O_3/TiO_2	3.5×10^{20} [c]	15	18	4.3	5.1
Fe_2O_3/Al_2O_3	1.5×10^{21} [c]	22	30	1.5	2.0

Note. Data source: Fe-HMS and Fe-MCM-41 (this work), Delam. Fe_2O_3-PILC and Fe_2O_3-PILC (Ref. 3), Fe_2O_3/TiO_2 and Fe_2O_3/Al_2O_3 (Ref. 2).

[a] Measured by neutron activation analysis.

[b] Assuming 100% dispersion for Fe^{3+}.

[c] Calculated from surface area, assuming surface fully covered by Fe_2O_3.

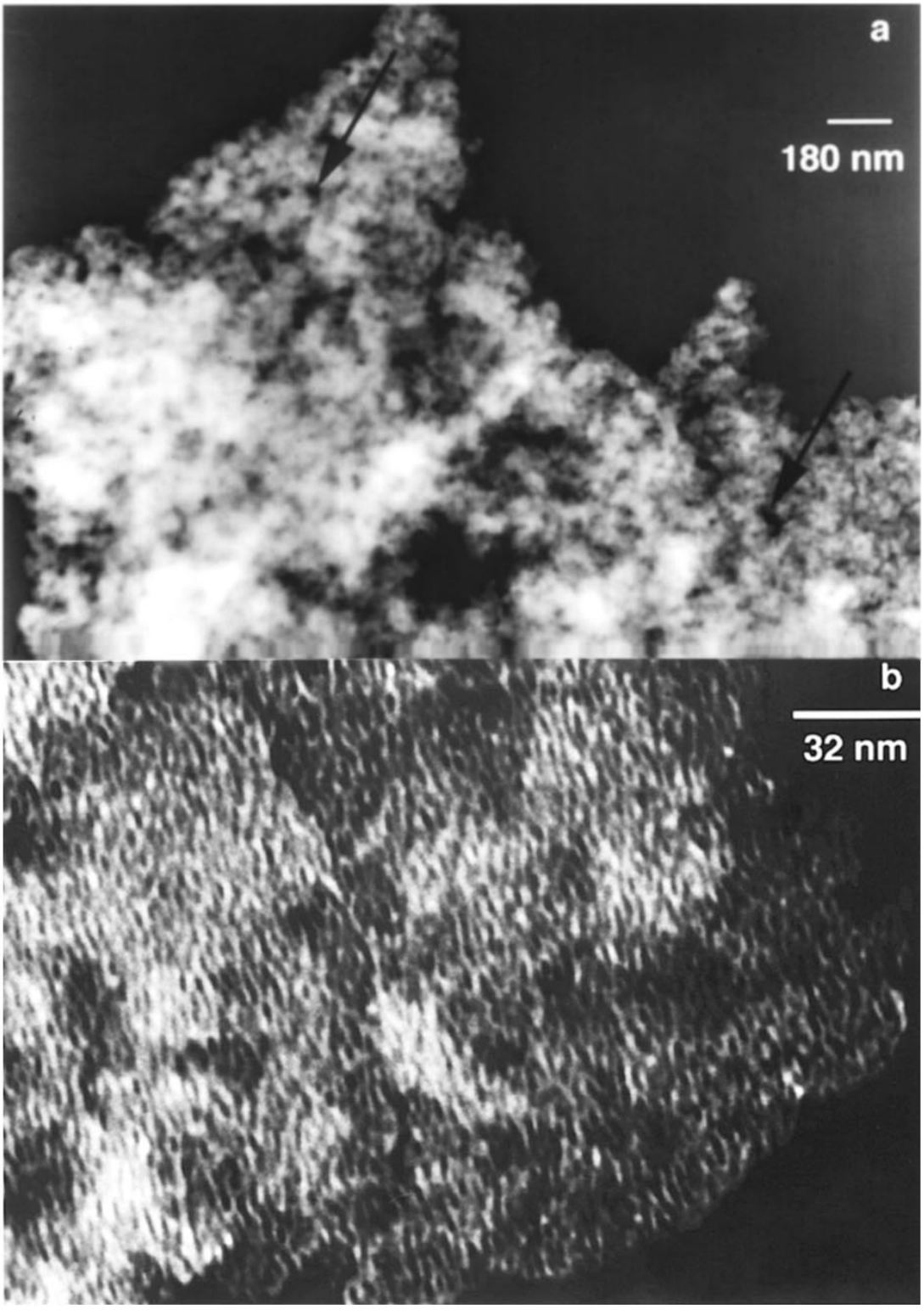

FIG. 2. TEM images for Al-HMS showing (a) the textural mesopores at a lower magnification and (b) mesopores at a higher magnification. Textural mesopores were absent from the TEM images of Al-MCM-41 (not shown).

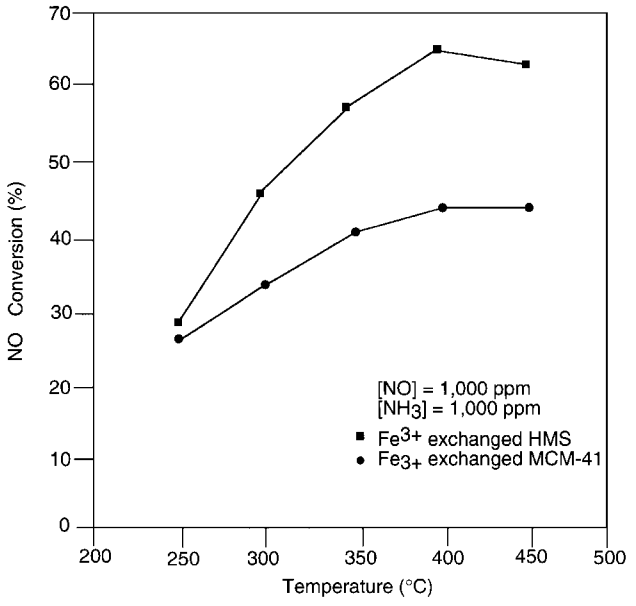

FIG. 3. Temperature dependence of the selective catalytic reduction of NO with NH_3 over Fe^{3+} exchanged Al-HMS and Al-MCM-41 catalysts. Reaction conditions: $[NO] = [NH_3] = 1000$ ppm, $[O_2] = 2\%$, in helium, total flow rate = 500 ml/min, catalyst weight = 0.4 g.

PORE DIFFUSION RESISTANCE

Results in Table 2 show that the Fe/Al-MCM-41 and Fe/Al-HMS catalysts were more active than the other Fe_2O_3 catalysts, on a per Fe^{3+} site basis. For example, at 350°C the apparent rate constant was 16.2×10^{-20} $cm^3/Fe^{3+}/s$, which was substantially higher than that for the other four catalysts. The high activity could be partly due to chemical reasons, e.g., the SCR activity is known to correlate with the Brønsted acidity for the V_2O_5-based catalysts (16). However, a more convincing reason for the differences in the apparent rate constants was the differences in the pore diffusion resistances. The pore dimension in the Fe_2O_3-PILC was of the order of 10 Å, whereas that in the delaminated Fe_2O_3-PILC was as large as about 20 Å (18). The pore dimension in the MCM-41 and HMS was about 28 Å. The large pore dimension could be interpreted as the main reason for the high activity. Moreover, the pores in the MCM-41 and HMS samples were uniform in size. The other catalysts had constrictions in the pore structure due to nonuniformity in the pore size distribution. These constrictions could be the limiting factor for pore diffusion. This could be the case with the Fe_2O_3/TiO_2 for Fe_2O_3/Al_2O_3 catalysts. Wong and Nobe noted that there was pore diffusion limitation in these catalysts, and effectiveness factors ranging from 16 to 95% were reported (2). Based on the above discussion, it is reasonable to conclude that the high activities in the Fe^{3+}-MCM-41 and the Fe^{3+}-HCM catalysts were due to a low diffusion resistance in their uniform pores.

HMS VS MCM-41: INTRINSIC TURNOVER FREQUENCIES AND PORE DIFFUSIVITIES

Although HMS and MCM-41 are similar both structurally and chemically, Fe/Al-HMS showed considerably higher activities than Fe/Al-MCM-41, as seen in Table 2. The framework pore dimensions, based on the Horvath–Kawazoe model with N_2 adsorption at 77 K, were 27 and 29 Å, respectively. The main differences between HMS and MCM-41 are the crystal domain sizes and the unique textural porosity of HMS. The crystal domain size for HMS was of the order 150 Å, whereas that of MCM-41 was larger by two orders of magnitude.

Assuming the same intrinsic rate constant (on per Fe^{3+} site) and pore diffusivity for Fe/Al-HMS and Fe/Al- MCM-41, it is possible to calculate these values from the apparent rate constants. The exact solution of Thiele (21) relating overall rate constant and intrinsic rate constant for first-order reactions is used in the calculation. The apparent rate constant, k_a (as used in Eq. [2]), is related to the intrinsic rate constant (k) by

$$\text{Rate} = k_a[NO] = k\varepsilon[NO] \qquad \text{or} \qquad k_a = k\varepsilon, \qquad [3]$$

where [NO] is the concentration of NO outside the pores, and ε is the effectiveness factor. The effectiveness factor is given by

$$\varepsilon = \tanh\left(L\sqrt{\frac{k}{D}}\right)\Big/\left(L\sqrt{\frac{k}{D}}\right), \qquad [4]$$

where L is the pore length and D is the pore diffusivity.

The apparent rate constants shown in Table 2, with units of cm^3/s/site, need to be converted to the units 1/s. The conversion factor is the number of Fe^{3+} sites per volume of pore space. The pore volumes were: 0.62 cm^3/g for HMS and 0.75 cm^3/g for MCM-41. The converted rate constants, or turnover frequencies, are given in Table 3.

The intrinsic turnover frequencies (k) and pore diffusivities (D) are calculated for Fe/Al-HMS and Fe/Al-MCM-41 at two temperatures and are shown in Table 3.

TABLE 3

Intrinsic First-Order Rate Constant (k) and Overall Diffusivity (D) for Fe^{3+} Ion Exchanged Al-HMS and Al-MCM-41

	Apparent k (s^{-1})		Intrinsic k (s^{-1})		Diffusivity (cm^2/s)	
Catalyst	350°C	400°C	350°C	400°C	350°C	400°C
Fe/Al-HMS	56.5	87.5	56.6	87.6	3.95×10^{-7}	4.0×10^{-7}
Fe/Al-MCM-41	30.0	38.5				

Note. The diffusivity and the intrinsic rate constants are assumed to be the same for both mesoporous catalysts.

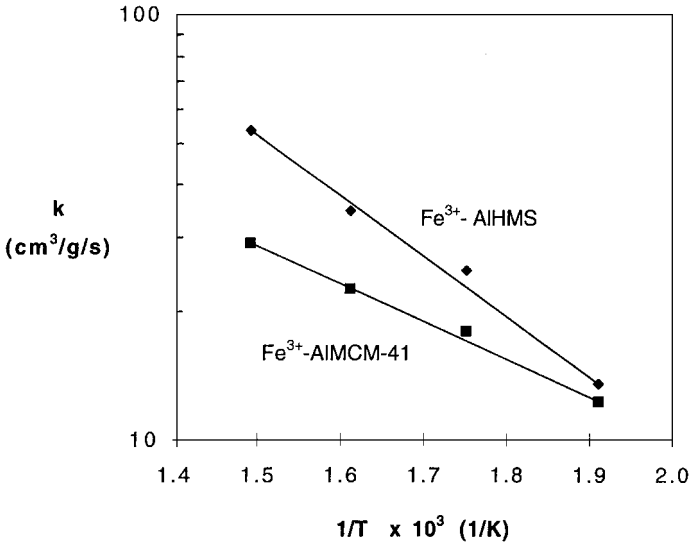

FIG. 4. Arrhenius plot for apparent rate constant, *k*.

The pore diffusivities are approximately 4×10^{-7} cm^2/s. The dimension of the actual free space is about 20 Å since NH_4^+ ions are adsorbed on the surface during the reaction (1). In the diffusion process, NO, NH_3, and O_2 reactant molecules diffuse in, while H_2O and N_2 product molecules diffuse out, forming a counterdiffusion system. It is known that diffusivities in micropores are substantially reduced by counterdiffusion (22). Thus the values shown in Table 3 are reasonable values. The results in Table 3 also show that the reaction in the Fe/Al-MCM-41 sample was severely limited by pore diffusion, but not for HMS. This may be due to the small domain size and textural porosity of HMS, which has been found useful for catalysis (23).

The effectiveness factor for the HMS zeolite was nearly 100%, whereas that for the MCM-41 zeolite was 0.53 at 350°C and 0.44 at 400°C. Arrhenius plots for the apparent rate constants are shown in Fig. 4. It is clear that combustion of ammonia was not significant at 400°C for both catalysts. The overall activation energy of 6.5 kcal/mol for Fe-HMS was in the range for SCR without diffusion resistance (1) and that of 4.0 kcal/mol for Fe-MCM-41 was in the range for SCR with diffusion limitation (1). The reason for the high effectiveness factor for the HMS catalyst lied in its small domain size (or short diffusion path). The advantage for the Fe^{3+} exchanged mesoporous molecular sieves, in particular Al-HMS, for the SCR reaction is clearly shown in this work. Furthermore, this work has demonstrated the importance of pore diffusion resistance in the NH_3 SCR reaction.

ACKNOWLEDGMENT

This work was funded by U.S. Department of Energy DE-FG22-96PC96206 to Ralph T. Yang and by National Science Foundation Grant CHE-9633798 to Thomas J. Pinnavaia.

REFERENCES

1. Bosch, H., and Janssen, F., *Catal. Today* **2**, 369 (1988).
2. Wong, W. C., and Nobe, K., *Ind. Eng. Chem. Prod. Res. Dev.* **25,** 179 (1986).
3. Chen, J. P., Hausladen, M. C., and Yang, R. T., *J. Catal.* **151**, 135 (1995).
4. Pinnavaia, T. J., *Science* **220**, 365 (1983).
5. Yang, R. T., Chen, J. P., Kikkinides, E. S., Cheng, L. S., and Cichanowicz, J. E., *Ind. Eng. Chem. Res.* **31**, 1440 (1992).
6. Cheng, L. S., Yang, R. T., and Chen, N., *J. Catal.* **164**, 70 (1996).
7. Kresge, C. T., Leonowicz, M. E., Roth, W. J., Vartuli, J. C., and Beck, J. C., *Nature* **359**, 710 (1992).
8. Beck, J. S., Vartuli, J. C., Roth, W. J., Leonowicz, M. E., Kresge, C. T., Schmitt, K. D., Chu, C. T.-U., Olsen, D. H., Shepperd, E. W., McCullen, S. B., Higgins, J. B., and Schlenker, J. L., *J. Am. Chem. Soc.* **114**, 10834 (1992).
9. Beck, J. S., U.S. Patent 5,057,296 (1991).
10. Chen, C.-Y., Burkett, S. L., Li, H.-X., and Davis, M. E., *Microprous Mater.* **2**, 27 (1993).
11. Feuston, B. P., and Higgins, J. B., *J. Phys. Chem.* **98**, 4459 (1994).
12. Luca, V., MacLachlan, D. J., Bramley, R., and Morgan, K., *J. Phys. Chem.* **100**, 1793 (1995).
13. Tanev, P. T., Chibwe, M., and Pinnavaia, T. J., *Nature* **368**, 321 (1994); Tanev, P. T., and Pinnavaia, T. J., *Chem. Mater.* **8**, 2068 (1996).
14. Horvath, G., and Kawazoe, K. J., *J. Chem. Eng. Jpn.* **16**, 470 (1983).
15. Spence, J. C. H., "Experimental High-Resolution Election Microscopy," p. 264. Oxford Univ. Press, New York, 1988.
16. Chen, J. P., and Yang, R. T., *J. Catal.* **125**, 411 (1990).
17. Chen, J. P., and Yang, R. T., *Appl. Catal.* **80**, 135 (1992).
18. Pinnavaia, T. J., Tzou, M. S., Landau, S. D., and Raythatha, R., *J. Mol. Catal.* **27**, 195 (1984).
19. Xie, Y. C., and Tang, Y. Q., *Adv. Catal.* **37**, 1 (1990).
20. Tanev, P., and Pinnavaia, T. J., *Science* **267**, 865 (1995).
21. Thiele, E. W., *Ind. Eng. Chem.* **31**, 916 (1939).
22. Chen, Y. D., Yang, R. T., and Uawithya, P., *AIChE J.* **40**, 4 (1994).
23. Zhang, W., Froba, M., Wang, J., Tanev, P., Wong, J., and Pinnavaia, T. J., *J. Am. Chem. Soc.* **118**, 9164 (1996).